

Online ISSN: 3009-7312
Print ISSN: 3009-6391

EJCBR

EGYPTIAN JOURNAL OF CANCER
AND BIOMEDICAL RESEARCH

<https://jcbr.journals.ekb.eg>

Editor-in-chief

Prof. Mohamed Labib Salem, PhD

Developing a magnetite/mesoporous silica core/shell system for enhancing the anti-cancer performance of doxorubicin at low doses for breast cancer treatment

Abdelhamid M. El-Sawy, Hoor M. Azab, Amal S. El-Shal, Sally M. Shalaby, Mohamed Y. El-Sheikh, El-Zeiny M. Ebeid, and Sherif M. Shawky



PUBLISHED BY

EACR EGYPTIAN ASSOCIATION
FOR CANCER RESEARCH

Since 2014

Developing a magnetite/mesoporous silica core/shell system for enhancing the anti-cancer performance of doxorubicin at low doses for breast cancer treatment

Abdelhamid M. El-Sawy¹, Hoor M. Azab¹, Amal S. El-Shal², Sally M. Shalaby², Mohamed Y. El-Sheikh¹, El-Zeiny M. Ebeid¹, and Sherif M. Shawky^{3,4}

¹Chemistry Department, Faculty of Science, Tanta University, Egypt

²Medical Biochemistry Department, Faculty of Human Medicine, Zagazig University, Egypt

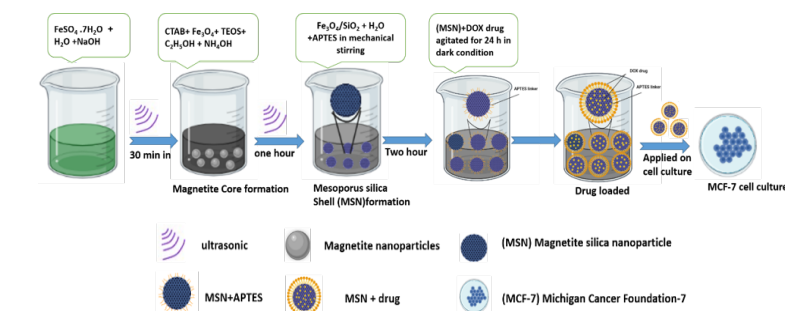
³Misr University for Science and Technology, Egypt

⁴Helmy Medical Institute, Center For Genomics, Zewail City of Science and Technology, Egypt

ABSTRACT

Background: Doxorubicin (DOX) is one of the main chemotherapies used in breast cancer in the form of many dosage forms such as encapsulation within pegylated liposomes and by injection. Both dosage forms have several side effects, most importantly dilated cardiomyopathy, erythema, acral erythema, and others. Also, DOX acquires resistance in dose-dependent manner by time. Consequently, there is an urgent need for novel approaches and strategies to improve current chemotherapeutic agents' delivery systems including DOX. Nanoparticles (NPs) have found their way in almost all aspects of biomedical applications within the last two decades, such as medical diagnostics, imaging, and drug/gene delivery systems. Mesoporous silica NPs are of great interest as an efficient drug/gene delivery system due to their unique properties. In the same context, magnetic nanoparticles contributed significantly to biomedicine, for their apparent features emerging at the nanoscale. Core/shell nanoparticles have potential characteristics as they incorporate the multiple merits of the used nanoparticles. **Aim:** Herein, we aimed at developing multifunctional sonochemical method for breast cancer treatment. **Materials and Methods:** Iron oxide/mesoporous silica/amino; core/shell (*M@silica/Amino*) was loaded with DOX as a drug delivery system (DDS). The synthesized multifunctional loaded/unloaded DDS was characterized by using TEM, SEM, XRD, FTIR, and TGA. Loading efficiency and release were measured and assessed using different models. Ultra-sonication was applied as external-stimuli of drug release from drug-loaded magnetite silica nanoparticles (*M@silica*). Evaluation of *M@silica@Amino@DOX* system as a nanoscale drug delivery system has been performed regarding safety, payload release, and efficiency of *in vitro* anti-cancer activity on MCF-7, and normal control MCF10A cell lines. Three time points intervals (1, 4 and 7 days) in triplicate were used to compare the maximum free DOX concentration that affects the cells viability. Molecular evaluation of the (*M@SiO₂@Amino@DOX*), (*M@SiO₂@Amino*), and (*free DOX*) was performed on the apoptotic biomarkers using real-time PCR as the main mechanism of action of DOX. **Results:** Potential achievements were obtained for the developed DDS concerning safety, dose adjustment, and mechanism of action compared to the free DOX. The data showed that the concentrations between 10 µg/ml to 25 µg/ml were safe to the cells and are currently applied to compare the effects of the DDS loaded with DOX and free forms regarding the best therapeutic effect, best time, in addition to, the ultra-sonication usage in drug release and/or treatment.

Keywords: Doxorubicin (DOX), Magnetic nanoparticles, Iron oxide/mesoporous silica/amino core/shell (*M@silica@Amino*), Drug delivery system and breast cancer, Cell lines



Editor-in-Chief: Prof. M. L. Salem, PhD - Article DOI: 10.21608/IJCBR.2024.236764.1315

ARTICLE INFO

Article history

Received: September 16, 2023

Revised: January 13, 2024

Accepted: March 31, 2024

Correspondence to

El-Zeiny M. Ebeid

Chemistry Department,

Faculty of Science,

Tanta University, Egypt

Tel.: +21155000056

Email:

elzeiny.ebeid@science.tanta.edu.eg

Copyright

©2024 Abdelhamid M. El-Sawy, Hoor M. Azab, Amal S. El-Shal, Sally M. Shalaby, Mohamed Y. El-Sheikh, El-Zeiny M. Ebeid and Sherif M. Shawky. This is an Open Access article distributed under the Creative Commons Attribution License, which permits unrestricted use, distribution, and reproduction in any format provided that the original work is properly cited.

INTRODUCTION

Cancer is a major global health problem. According to the WHO, more than 20 million new cases of various cancers have been aroused in 2020 with about 10 million deaths. Breast cancer (BC) is the top cancer type's cases among women in 2020 with more than two million diagnosed (24.5%), compared to other females' cancers. Furthermore, it is the highest top prevalence type within the last 5 years among women. BC treatment depends mainly on its type/subtype including but not limited to surgery, radiotherapy, and chemotherapy.

Cancer as a multifactorial disease is affected by diverse factors both internally (genetic factors) and externally (environmental factors as physical, chemical, biological like viruses) (WHO, 2021a). BC has the highest prevalence among women within the last five years, with about 25 million cases and more than 2 million in 2020, with 685k death globally (WHO, 2021a, WHO, 2021b)). Hence, various treatment protocols/ approaches are currently followed, including multiple chemotherapeutic agents, radiation, hyperthermia, immune and hormonal therapy. Despite being proven to be effective in many cases, the efficacy is almost in parallel with early diagnosis and the accompanying serious side effects by the above-mentioned approaches, especially chemotherapy (single and combined treatment).

DOX Chemotherapy is the main scope of this study. It suffers from many side effects, such as dilated cardiomyopathy. DOX, like other chemotherapeutic agents, is not specific and reaches almost all the body cells. Our driving force was to resort to coupling chemotherapy with a nanoparticles-based smart drug delivery system. Nanoparticles (NPs) have a broad spectrum of applications in biomedicine, such as drug delivery and medical diagnostics (Shawky et al., 2014). Magnetic nanoparticles (MNPs) possess unique properties which make them highly attractive to medical applications, such as high surface-to-volume ratio, specific quantum properties, biocompatibility, high super-magnetism, and ease of their surface modifications (Zada et al., 2016). Also, they have been recognized as prominent candidates

for drug delivery applications because they are "naturally" biocompatible (Xiao and Xiao, 2009).

On the other hand, mesoporous silica NPs are of great interest as an efficient drug delivery system due to their unique properties such as large surface area, tunable pore sizes, highly ordered structures in addition to their chemical and thermal stability. Mesoporous silica NPs also have high loading efficiency for both hydrophilic and hydrophobic molecules (Tasciotti et al., 2008, Torney et al., 2007). These features make them ideal for encapsulating different guest molecules and facilitate a wide range of applications, especially cell imaging and drug and/or gene delivery in animal and plant cells (Lai et al., 2003, Slowing et al., 2007)). Lot of studies have used mesoporous silica nanoparticles as DDS with or without magnetic nanoparticles with the main advantage of using the core magnetite in hyperthermia treatment along with the delivery of the drugs. Also, pH-responsive Mesoporous silica composites have shown promising results as DDS (Slowing et al., 2007, Keshavarz et al., 2020, Moorthy et al., 2017)). In one of our studies, we designed and synthesized smart mesoporous silica nanoparticles coated with pH-responsive polymer and showed highly efficient encapsulating anti-tuberculosis drugs using a rotary evaporator as a novel method for drug loading (Shawky et al., 2016b).

Despite the availability of many mesoporous-based DDSs established in the last decade for many drug molecules including DOX, mesoporous silicate as DDSs is still a hot topic research tool in biomedicine applications, aiming to achieve the superior DDS with minimal side effects and enhancement of its properties. In 2018, Hakeem et al. (Hakeem et al., 2018) have developed conventional MCM 41 Mesoporous silica nanoparticles and used DOX as a model drug using poly aspartic acid as the pH-responsive trigger in HepG2 Cell lines. Recently, Yan et al. have developed pH/Redox responsive mesoporous silicate nanoparticles for co-delivery of Dox and Paclitaxel for breast cancer treatment (Yan et al., 2020).

Moreover, Day et al. have developed MCM R1 Mesoporous silicate by Stober method for DOX and Tamoxifen delivery for breast cancer

treatment also based on pH-responsive cargo release depending on the high solubility of DOX at acidic pH.

Therefore, enhancing the properties of the mesoporous silicate nanoparticles alone or as a composite/core/shell is under continuous evaluation in the scientific community, and DOX is usually the best model chemotherapeutic agent to be used to its well-known serious side effects. So, developing DDS for DOX as a model with the aim of eliminating/minimizing side effects will be a turning point in the DDS in general and mesoporous silica nanoparticles specifically.

In this study, a multifunctional carrier has been designed for drug delivery composed of magnetic iron oxide (Magnetite core) using Ultra Sonication (Abbas et al., 2013), then coating by Mesoporous silica as a shell by a sonochemical method (Abbas et al., 2014, Banaei et al., 2015), decorated by amino groups using 3-Amino propyl- tri-ethoxy silane (APTES), and finally mechanical stirring has been used for loading DOX. Selecting the optimum dose of the prepared system, cell viability, and anti-cancer effect, in addition to accessing the molecular mechanism of DOX in MCF7 and MCF10A cell lines, has been achieved.

Mesoporous silica nanoparticles (MSNs) have been extensively used as encapsulating agents in drug delivery, diagnosis, and bioimaging. Nevertheless, concern about their biosafety *in vivo* was raised since silanol groups interact with the surface of the phospholipids of the red blood cell membranes resulting in hemolysis (Zhao et al., 2011). To minimize this side effect, we applied small concentrations between 10 µg/ml to 25 µg/ml to be safe to the cells. Moreover, extensive functionalization of the Fe₃O₄/SiO₂ (M@silica) core shell nanoparticles was performed at the expense of free silanol groups using 3-Amino propyl- tri-ethoxy silane (APTES) and Doxorubicin (DOX) drug to get Fe₃O₄@silica@ Amino @DOX drug delivery system (DDS).

EXPERIMENTAL

Materials

Iron (II) sulfate heptahydrate (FeSO₄.7H₂O), sodium hydroxide (NaOH), ethyl alcohol (C₂H₅OH), ammonia (NH₄OH, 0.25 M),

Tetraethylorthosilicate (TEOS), Cetyl-Trimethyl Ammonium Bromide (CTAB), phosphate buffer solution (PBS), and doxorubicin hydrochloride C₂₇H₃₀ClNO₁₁ (DOX) anti-cancer drug, 3-(4, 5-dimethylthiazol-2-yl)-2, 5-diphenyltetrazolium bromide (MTT) reagent (Sigma-Aldrich, St. Louis, MO, USA), 10% fetal bovine serum (FBS) (Lonza Bioproducts), the Detergent reagent (cat. number 4890-25-02) and 1% penicillin, streptomycin, Amphotericin B Mixture (Lonza Bio products), All chemicals were of analytical reagent grade and used as received without any further purification.

Characterization instruments

X-ray powder diffraction (GNR X-ray diffractometer/APD 2000 PRO) with Cu anode, line focus ($\lambda = 1.540562 \text{ \AA}$) in the 2 θ range from 10-90 with step size is 0.050. Fourier- transform infrared spectroscopy (FT-IR) (Thermo Nicolet FTIR Avatar 370). Thermogravimetric analysis was performed using the PerkinElmer TGA-50 apparatus.

For the TGA analysis, 7 mg of each sample was located separately in the TG instrument pan to record the weight residue with increasing temperature at a heating rate of 5 °C min⁻¹ under a nitrogen atmosphere with a gas flow of 10 mL min⁻¹.

The magnetization behavior was measured by hand-made vibrating sample magnetometer (VSM), Department of Physics, Faculty of Science, Tanta University in an external magnetic field ranging from -10 kOe to + 10 kOe (T.M. El-Alaily M.K. El-Nimr 2015). Ultrasonic instrument (DAIHAN-brand® Analog Ultrasonic Cleaners, WUC-A, with frequency 28/40 kHz and heating power is 172W).

Synthesis of magnetic iron oxide (Fe₃O₄)

In a typical synthesis, 2.31 gm of FeSO₄.7H₂O was dissolved in 90 mL distilled water for 10 min using a magnetic stirrer and then sonicated using an ultrasonic processor for 75 min. 9 mL of 3 M sodium hydroxide (NaOH) was injected in the reaction after 15 min of starting ultrasonication. The black precipitate of the produced Fe₃O₄ was washed five times in water and ethanol, followed by collecting the precipitate using a magnet and then dried in an oven at 80 °C overnight (Abbas et al., 2013).

Synthesis of Fe₃O₄/SiO₂ (M@silica) core shell nanoparticles

Four grams of CTAB were dissolved in 60 mL distilled water (D.W) then mixed with 100 mg of Fe₃O₄ dispersed in 20 mL D.W under ultrasonication for 30 min. Then 100 mL of absolute alcohol and 5 mL of ammonia were added, and sonication was continued for further 30 minutes. During ultra-sonication, 1.5 mL of TEOS was added to the solution. The solution was then washed several times with ethanol and water. The Fe₃O₄/SiO₂ (M@silica) precipitate nanoparticles were collected using a magnet, washed with water and alcohol and, then dried in an oven at 80 °C overnight (Shawky et al., 2016a, Abbas et al., 2015).

Functionalization of the core/ shell with APTES

0.5 mg of Fe₃O₄/SiO₂ (M@silica) was dispersed in 100 mL D.W, and then APTES (0.2 mL) was added under mechanical stirring. The reaction mixture was heated up to 70 °C for 2 hours then cooled down to room temperature, followed by magnetic decantation and thorough washing with ethanol. The samples were then dried in an oven at 60 °C for 24 h (Liu et al., 2013, Strand, 2016).

Anti-cancer drug loading (DOX loading)

For drug loading, DOX was dissolved in phosphate buffer saline (PBS, pH7.4) to obtain DOX solution with a concentration of 0.5 mg/ml. Subsequently, 60 mg of Fe₃O₄/SiO₂ (M@silica) nanoparticles were dispersed in 12 mL of the DOX solution. The mixture solution was agitated for 24 h under dark conditions and then collected by centrifugation to obtain the DOX-loaded Fe₃O₄/SiO₂ (Shahabi et al., 2015). Three concentrations (250, 500, and 1000 ppm) have been used for DOX loading for evaluating the loading efficiency percentage (Yu and Zhu, 2016, Unsoy et al., 2014).

$$\text{Drug Loading \%} = \frac{C_0 - C_s}{C_0} \times 100\% \quad (1)$$

Where C₀ is the drug concentration solution before loading and C_s is the concentration of the solution after loading.

FTIR Analysis

FTIR spectra of the samples were taken using the potassium bromide (KBr) pellet technique

for all samples including as-synthesized magnetite, magnetite/silica, magnetite/Silica/APTES, and magnetite/ silica/APTES/DOX.

Effect of ultrasonication on drug release

M@silica DOX-loaded drug carrier was allowed to release DOX drug under the influence of ultra-sonication. A constant weight of 60 mg M@silica loaded by DOX was dispersed into 10 mL buffer (pH = 7.7) and subjected to ultrasonication. The temperature of the drug carrier system was kept constant by replenishment of ambient water to avoid sample heating upon ultrasonication. The amount of drug release was measured by using UV-Vis spectrophotometer by measuring the absorbance at 490 nm every 20 min (Deng et al., 2016, Jain et al., 2018, Cheung and Neyzari, 1984).

In vitro drug release

Drug release has been studied in phosphate buffer saline (PBS) at two different pH values: 5.5 and 7.4 to mimic the endosomal vesicles and the blood pHs, respectively. Briefly, 60 mg DOX loaded particles were suspended in the buffer solutions. Then, the solution was stirred using mechanical stirring at 37°C, and aliquots were centrifuged for specific time intervals. The amount of drug release was measured by measuring the absorbance at 490 nm every 20 min, and the concentration was calculated from the calibration curves of the drug. The release percentage was calculated according to the following equation (Ellis et al., 2017, Unsoy et al., 2014).

$$\text{Drug Release \%} = \frac{C_t}{C_0} \times 100\% \quad (2)$$

Where: C_t is the concentration at a specific time, C₀ is the initial concentration.

Release kinetics of DOX from the prepared DDS

For better understanding, the drug release from the prepared DDS was studied at two pH values (7.5 and 5.5). The *in vitro* release of DOX has been analyzed by fitting to different kinetic model equations: zero-order (cumulative% drug release vs. time), first-order (log % drug remaining vs. time) and, Higuchi (cumulative % drug release vs. time square root). The release data obtained was treated according to Korsmeyer–Pappas (*log cumulative*

percentage drug release vs. log time) and the release exponent value (n) is calculated at the different pH values. To determine the correlation coefficients (R^2), the release rate constant was calculated. Consequently, the best fitting model is one of the highest R^2 values (Korsmeyer et al., 1983, Mhlanga and Ray, 2015, Gouda et al., 2017, Fu and Kao, 2010, T. Chatzēiōannou, 1993))

RESULTS AND DISCUSSION

Analysis of the morphology and size of different synthesized DDS components

SEM images for magnetite formed by the sonication method are shown in Figure 1. The images showed the formation of a uniform spherical nanoparticle with an average size of 25 ± 5 nm. The magnetite silica (M@silica) nanoparticles were recorded in Figure 1 (A) and (B). The surface morphology shows the presence of the drug on its surface as small white dots with no aggregation for the particles been observed. The average size for magnetite silica nanoparticles (M@silica) after functionalization with APTES and loading with the drug was about 140 ± 50 nm. Transmission electron microscopy (TEM) images Figure 2. Showed the formation of magnetite silica nanoparticles in a uniform spherical shape (Figure 2A) distinctly, in addition to the uniform size of the core/shell (Figure 2B). Moreover, with zooming the core/shell (Figure 2C), the shell pores are shown clearly to surround the magnetite nanoparticles and another layer of functionalized APTES is found also. The core magnetite radius is about 25 ± 5 nm, and the (silica, APTES) shell thickness is about 107 ± 45 nm. The whole core-shell size of magnetite silica is 140 ± 50 nm approximately. (TEM) images obviously showed the formation of magnetite silica nanoparticles in a spherical shape. It also showed the uniform size of the core-shell.

Average of particles size

The size distribution of magnetite nanoparticles which were synthesized using the sonochemical method ranges from 18 to 30 nm. The size distribution of magnetite particles after loading with silica and drug in TEM and SEM imaging, the particle size distribution ranging from 100 to 200 nm.

(TEM) was used to confirm the formation of $Fe_3O_4@SiO_2$ core-shell nanoparticles. The TEM images demonstrate that the NPs have a core-shell structure with light contrast silica shells and dark contrast cores of Fe_3O_4 due to density difference, implying that the Fe_3O_4 was coated by a silica shell. (TEM) was used to confirm the formation of $Fe_3O_4@SiO_2$ core-shell nanoparticles. The TEM images demonstrate that the NPs have a core-shell structure with light contrast silica shells and dark contrast cores of Fe_3O_4 due to density difference, implying that the Fe_3O_4 was coated by a silica shell.

Energy dispersive X-ray (EDX) analysis

The presence of silica was confirmed using Energy dispersive X-ray (EDX) analysis. Energy dispersive X-ray (EDX) measurements indicate that iron and silica are present with weight percentage 8.79% and 20.02% respectively. The small white dots on the SEM images are rich in carbon, oxygen and nitrogen and accordingly represent the loaded DOX drug. The weight percentages of C, N and O are 19.76%, 7.37% and 44.06%, respectively. The high percentage of carbon and oxygen in comparison with Si and Fe is due to the existence in both APTES and DOX drug (Asab et al., 2020).

XRD Patterns of the magnetite and the magnetite/silica core/shell

Magnetite /silica (M@silica) nanoparticles were analyzed by (XRD). XRD patterns for both Fe_3O_4 nanoparticles and Fe_3O_4/SiO_2 core-shell nanoparticles. The diffraction peaks of the Fe_3O_4 nanoparticles correspond to the crystal planes of (111), (311), (400), (422), (511), and (440), which indicate the formation of a fully crystalline and pure phase of magnetite with a cubic inverse spinel structure. The position and relative intensity of all diffraction peaks match well with those of the magnetite (JCPDS 19-629), and the broad peaks indicate their monocrystalline nature. The crystallite size was determined using the Scherrer Equation from the most intense peak, and it was equal to 30 nm (Kalantari et al., 2017). The XRD pattern of silica-coated Fe_3O_4 magnetic nanoparticles showed broad diffraction at $2\theta=10-20^\circ$, suggesting an amorphous structure of the mesoporous silica coating.

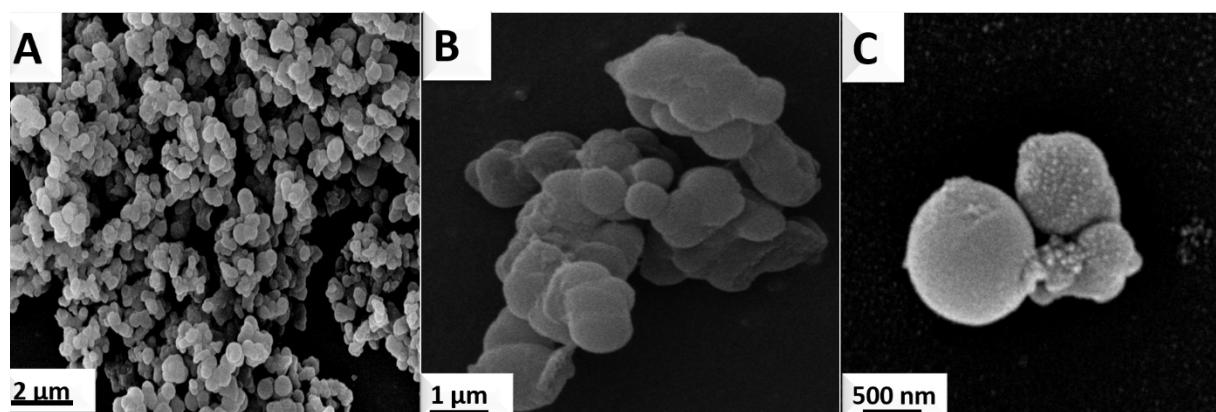


Figure 1. Scanning Electron Microscope (SEM) images for (A and B) magnetite silica nanoparticles M@silica at low and high scales. (C) The as synthesized magnetite nanoparticles (Fe_3O_4).

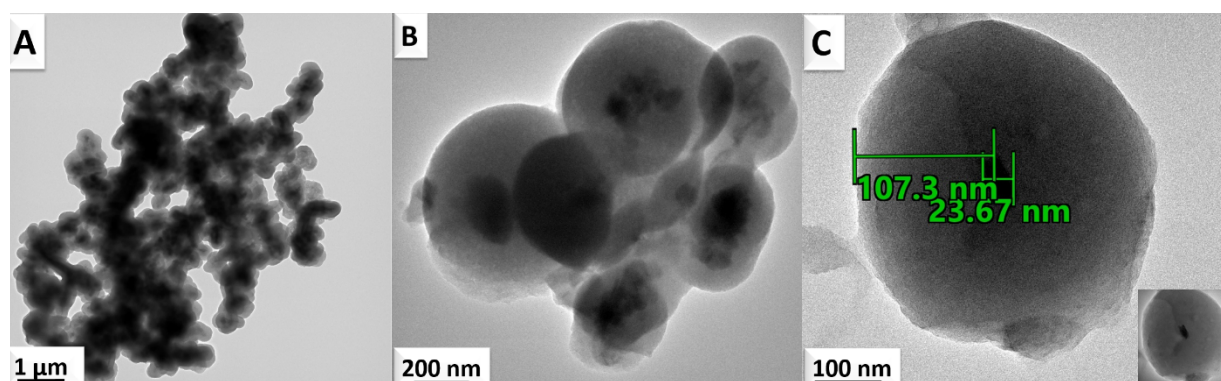


Figure 2. Transmission Electron Microscope (TEM) images of the DDS and its components showing; (A) as synthesized magnetite nanoparticles. (B), and (C) showing magnetite mesoporous silica nanoparticles core shell (M@silica) at different scale bars.

The other diffraction peaks were the same as those of magnetite nanoparticles, indicating that the crystal structure of the magnetite nanoparticles did not change after the coating of mesoporous silica and the removal of surfactant (Pattnaik, 2011). The broad peak at $\theta = 12^\circ$ in XRD pattern is not the only one that proves the presence of silica. The interplanar distance did not change for magnetite after coating with silica, which means that silica is only present on the surface and not doped in the crystal structure of the magnetite core.

FTIR and Magnetization of the delivery system components

FTIR has been used to retrieve the different functional groups of the prepared nanomaterials (Ullah et al., 2014). The peaks at 595 cm^{-1} , 1460 cm^{-1} and 1630 cm^{-1} can be showed in all three FTIR spectra, which were characteristic of Fe–O vibrations within the magnetic core, Fe–O stretching within magnetite core and the stretching of the solvent

hydroxyl groups (OH), respectively. Silica coating has revealed the main bands of absorption at 775 cm^{-1} and 471 cm^{-1} associated with Si–O bending and Si–O–Si bending respectively, along with the characteristic signal at 1063 cm^{-1} ascribed to asymmetric Si–O–Si vibration or Si–O–Fe stretching vibration in the silica shell. These absorption bands clearly demonstrated silica coating of the magnetite surface. The N–H bending vibration of primary amines is observed in the region $1650\text{--}1580\text{ cm}^{-1}$. The bending vibrations of amino groups were detected at 1644 cm^{-1} , meaning that amino groups have been loaded on the surface of silica coating. Functionalization of silica by amino propyl was further confirmed by the presence of C–H stretching vibration observed at $2800\text{--}3025\text{ cm}^{-1}$ and 3450 cm^{-1} is for O–H bond. After drug loading, the FTIR spectra showed a peak at 2900 cm^{-1} that is assigned to C–H bond stretching confirming the DOX drug loading (Sun et al., 2015). The magnetic hysteresis loops of the prepared magnetite/silica core-shell

nanoparticle samples showed that the samples were measured at room temperature using VSM in an external magnetic field ranging from -10 kOe to $+10$ kOe. The saturation magnetization value, extracted from the corresponding hysteresis loop, for the uncoated magnetite/silica sample, was 36.46 emu/g. The saturation magnetization value decreased after coating the core shell with APTES reaching 12.15 emu/g. Further decrease was observed after loading the drug to become 8.9 emu/g. The decrease in the magnetization value after each step in all the samples, is normal due to the incorporation of nonmagnetic silica shell around the core magnetite nanoparticles, APTES and DOX. Furthermore, reduction in the magnetization value following silica coating due to the formation of chemical bonds such as (Fe-O-Si), between the Fe ions particularly at the surface with silica, resulting in partial disappearance of the Fe ions magnetic moment. Interestingly, the relatively high magnetization value of 36.46 emu/g is favorable for many applications, especially the targeted drug delivery applications which require magnetic nanoparticles of high magnetic moments for easy manipulation (Abbas et al., 2014). The shift in the hysteresis loop causes a coercive field (H_c) change when the ferromagnetic and antiferromagnetic systems are cooled in a magnetic field. Episodes in hysteresis depend on cooling of the field value and the temperature. The coercivity and exchange bias fields were calculated from the M-H (magnetization versus applied magnetic field) hysteresis loops. The coercivity can be calculated using Eq. (3). The coercivity (H_c) and remanence values decreased from (114 Oe, 6.36 emu/g) respectively for the magnetite/silica core shell to 111 Oe, 4.58 emu/g for magnetite /silica /APTES and 97.5 Oe, 3.03 emu/g for magnetite silica /APTES/drug. This decrease in coercivity value after loading APTES and drug may be due to the lower specific absorption rate (SAR) of the other two samples. Moreover, these layers reduce magnetic dipole coupling interactions between adjacent magnetic nanoparticles, and thus reduce the coercivity value of hysteresis loops measurements. The exchange bias is obtained by measuring the shift in the M-H hysteresis loop along the horizontal and vertical direction.

The exchange bias field (H_{EB}) is obtained by the horizontal shift in the hysteresis loops, H_{EB} . The exchange bias field, H_{EB} was calculated using the following Eq. (4) (Narayanaswamy et al., 2022).

$$H_c = \frac{|H_{c1} - H_{c2}|}{2} \quad (3)$$

$$H_{EB} = \frac{|H_{c1} + H_{c2}|}{2} \quad (4)$$

The behavior of exchange bias showed a positive exchange bias in magnetite silica and a negative exchange bias for the sample after functionalized with APTES and loading drug.

Thermogravimetric analysis (TGA) and loading efficiency

TGA was utilized to evaluate the drug loading efficiency in the DDS according to mass change (weight) of the sample as a function of temperature and supported by studying of DTGA. The thermograms of the loaded DOX, compared to Magnetite/ silica and magnetite/silica/APES samples starting from ambient temperature to 700 °C. From the derivation of TGA for three TGA curves, the major loss in weight at temperature between $30-160$ °C due to evaporation of water and ethanol solvents. In $Fe_3O_4/SiO_2/APTES$ curve, there were two stages for the weight loss stage one at temperature between $30-150$ °C which attributed to water and ethanol solvents and stage two at temperature between $160-500$ °C due to thermal decomposition of organic component belongs to APTES. In $Fe_3O_4/SiO_2/APTES/drug$ curve the weight loss happened at three stages, stage one at temperature between $30-150$ °C which attributed to water and ethanol solvents, which was about 12.5% in the DOX loaded particles. Stage two at temperature between $160-500$ °C due to thermal decomposition of organic component belongs to APTES, which was about 4.94% and stage three at a temperature above 500 °C belongs to thermal decomposition of drug components, which was about 10.1% . Therefore, starting from 160 °C till 700 °C, weight loss corresponds to the covalently attached APTES and DOX between each other and to the silica nanoparticles. Consequently, the percentage of the drug (DOX), could be calculated from the weight loss from 160 °C to 700 °C in both samples (Iron/Silica/APTES) and

(Iron/Silica/APTES/DOX) considering the weight loss occurring in drug-loaded and unloaded particles. The weight loss from 160 to 700% in the DOX loaded particles was about 15% and for the unloaded particles was about 18.99%. After calculating the different weights and the weight losses, it was found that there are 4 μ g DOX per mg iron/silica particles, which is about 0.06 μ mol Doxorubicin (Qiao et al., 2015).

The loading of the DDS by DOX was highly affected by the DOX drug concentrations used in the experiments. It was found that by increasing DOX concentration from 250 to 500 ppm (0.25 to 0.5 mg/ml), the loading efficiency has been increased from 43% to 86%. Upon increasing the concentration to 1000 ppm (1 mg/ml), loading efficiency decreased to 63%. Consequently, 500 ppm has been used for the DOX loading to achieve the maximum loading of the drug. Therefore, the amount loaded of drug per the DDS, was 5.16 mg DOX/60 mg particles, which is equals to 86 μ g DOX/mg DDS, and 86 ng DOX/ μ g DDS. As the Molecular weight of Doxorubicin hydrochloride is: 543.52 g/mol, so, the μ g of the DDS contains about 0.158 μ mol DOX (0.158 μ mol/ μ g DDS).

Evaluation of the *in vitro* drug release patterns

The *in-vitro* release data at two pHs (5.5 and 7.4) were analyzed using different models to determine the release model that best describes the DOX release from the DDS and summarized in Table 1. By comparing the R^2 values, it was found that the DDS at pH: 5.5 follows the Korsmeyer-Peppas model with *diffusion exponent value* $n = 0.11$, indicating that the drug release at acidic media (pH = 5.5) is Fickian diffusion. On the other hand, at pH = 7.4, the release pattern fits zero-order release as it has the highest $R^2 = 0.90$, and also follows Fickian diffusion as $n = 0.28$ (If $n \leq 0.45$, release diffusion-controlled (Fickian diffusion) (T. Chatzēiōannou, 1993). Hence, the release pattern of the DOX from the silica/APTES nanoparticles depends on the diffusion of the drug only not the erosion of the silica nanoparticles. The pH effect on the drug release showed a large amount of the drug was released within a very short time at the acidic pH, compared to the neutral pH. This could be explained by the hydrolysis of the imine bond

formed between the APTES protonated amino group and the DOX carbonyl group, by decreasing the pH, the hydrolysis of the imine bond is enhanced yielding the free DOX and the primary amine of the APTES. This effect mimics the internalization of the particles by the endosomal vesicle, where the pH is around 5.5, and so the presence of the protons and other counter ions in the endosomal vesicle will lead to filling up the pores of the particles with them in addition to, hydrolysis of the DOX, and protonation of the amino group on APTES and the other one on the DOX. Collectively, the endosomal vesicle will rupture, and the DDS will be released in the cytoplasm, along with the drug.

Kinetics of drug release by using ultra-sonication

The stimulated drug release data under the influence of ultra-sonication was analyzed using different models to determine the release model that best describes the DOX release from the DDS. By comparing the R^2 values, it was found that the DDS, at pH=7.4, the release pattern fits Higuchi release as it has the highest $R^2=0.96$, and also follows Fickian diffusion as $n=0.35$ (If $n \leq 0.43$, release diffusion-controlled Fickian diffusion) (Figures 3, 4) (T. Chatzēiōannou, 1993). Hence, the release pattern of the DOX from the silica/APTES nanoparticles depends on diffusion of the drug only not erosion of the silica nanoparticles. By comparing releasing of the drug by mechanical method with releasing by sonication method, we found that sonication method is five time faster than mechanical method as sonication release the same amount of drug in time = 1/5 time in mechanical stirring.

Cytotoxicity evaluation of the prepared drug-free delivery system

The cytotoxicity effect of the drug-free delivery system on normal breast cell lines is summarized in Table 2 and shown in Figure 5. There was non-significant difference between MCF10A-cells incubated with the DDS (magnetite silica nanoparticle) at 10 μ g DDS/ml concentration and the normal cell line (control samples) in day 1 ($p = 0.42$), day 4 ($p = 0.47$) and day 7 ($p=0.59$) which means that the particles have no cytotoxicity effect at 10 μ g/ml concentration.

Table 1. Controlled release kinetics of DOX drug from DDS nanoparticle at pH = 7.4 and 5.5.

Magnetite/silica/APTES/DOX	Zero order		First order		Higuchi Model		Korsmyer-Peppas Model		
Parameter	R ²	K ₁	R ²	K ₂	R ²	K ₃	R ²	K ₄	n
pH = 7.4	0.90	0.22	0.78	-0.006	0.88	3.2	0.89	1.2	0.28
pH = 5.5	0.92	0.85	0.89	-0.004	0.82	1.26	0.96	1.6	0.11

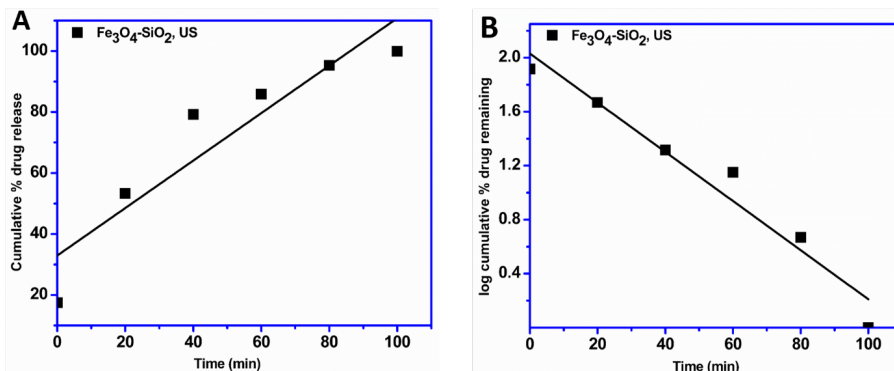


Figure 3. (A) Zero order model, (B) first order model for magnetite silica by using ultra-sonication.

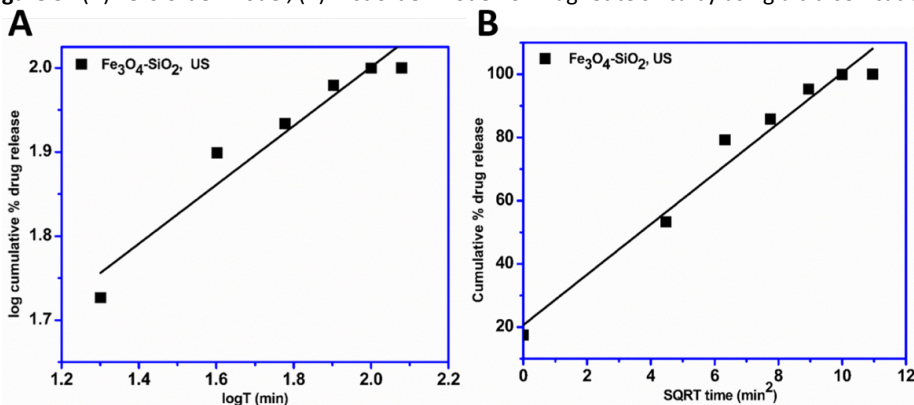


Figure 4. (A) Korsmeyer- Peppas model, and (B) Higuchi model by using ultra-sonication.

Table 2. cytotoxicity effects of the drug delivery system

	Cell viability %		
	Day 1	Day 4	Day 7
MCF10A cells only (control)	99.87±0.34	99.65±0.36	99.55±0.65
MCF10A-cells +delivery system (10 µg/ml)	99.23±0.42	98.87±0.47	98.83±0.59
MCF10A-cells +delivery system (20 µg/ml)	83.14±0.57	79.06±0.63	81.23±0.75
MCF10A-cells +delivery system (40 µg/ml)	76.38±0.33	68.95±0.42	73.17±0.54

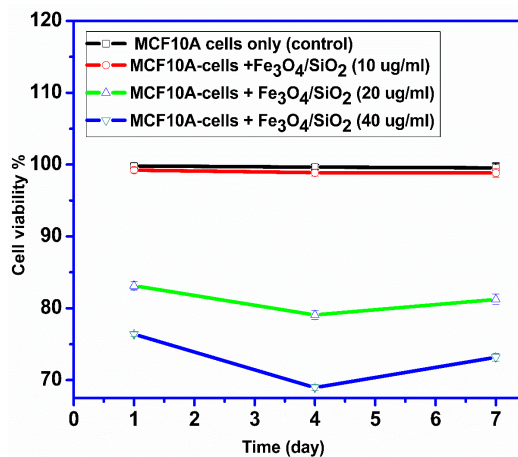


Figure 5. The evaluation of the different concentrations of the DDS on normal MCF10A cells viability. As shown, there is almost no effect on cells at DDS 10 µg/ml.

On the other hand, there was a significant difference between MCF10A-cells/DDS at concentrations 20 µg/ml and 40 µg/ml, compared to the control samples on days 1, 4, and 7 ($p < 0.001$). Based on these data, the subsequent experiments have been done using the drug delivery system at concentration 10 µg/ml.

***In-vitro* Anticancer assay**

MCF-7 cells were treated with free DOX at different concentrations (2-10 µM) and compared with the DOX drug delivery system at concentration 10 µg/ml, for 48 hours. It was found that there was a significant decrease of cell viability percentage in a dose-dependent manner either for the cells treated with free DOX or cells treated with DOX-loaded DDS. Moreover, there was a significant effect of DOX/Silica on MCF-7 when compared to DOX only ($p < 0.001$). The data is summarized in Table 3 and in Figure 6. Interestingly, the amount of Doxorubicin in the particles was about 0.086 ng, with a final concentration of 1.58 µM.

The same results have been shown when studying the effect of DOX at different time intervals on cell viability as there was a significant decrease of cell viability percentage in a time-dependent manner. The highest effect was about 49% by DOX loaded on the magnetite silica nanoparticles in day 7, as shown in Table 4 and Figure 7.

Effect of the studied drug on apoptotic process

The study showed that DOX induced apoptosis by up regulating Bax, and down regulating anti-apoptotic Bcl2 gene expression. The apoptotic effect was significantly higher in MCF-7 cells treated by DOX loaded on silica particles than in cells treated by free DOX only (Figure 8, Table 5).

CONCLUSION

In this study, a drug delivery system has been synthesized by ultra-sonication, the system is composed of magnetite/mesoporous silica core/shell system, functionalized with APTES and then, loaded with doxorubicin, as a chemotherapeutic agent used for the treatment of breast cancer. The developed system has a core-shell structure with a radius equal to 210 ±

30 nm and a structure with a higher magnetization value equal 36.46 emu/g. Magnetite silica nanoparticles had the same drug release behavior with two different pH, in pH 7.4 and 5.5 (when mechanical stirring is applied).

The system flow zero-order model and Korsmeyer-Peppas model with higher $R^2 = 0.90$ and 0.96, respectively. Upon using ultrasonic as an external stimulus, the system showed some difference as the drug releasing became higher five time more than mechanical stirring, and the system follows Higuchi model rather than other models. There was non-significant difference between MCF10A-cells + delivery system (magnetite silica nanoparticle) at concentration 10 µg/ml and the normal cell line (control samples) in day 1 ($p = 0.42$), day 4 ($p = 0.47$) and day 7 ($p = 0.59$) meaning that there was no cytotoxicity effect when the drug delivery system at concentration 10 µg/ml. The study showed that DOX induced apoptosis by upregulation Bax, and down regulating anti-apoptotic Bcl2 gene expression. The apoptotic effect was significantly higher in MCF-7 cells treated by DDS loaded with DOX than in cells treated by free DOX only. Interestingly, the cell viability has decreased to 55% after two days-incubation with DDS at concentration 10 µg/ml, which contains almost 1.8 µM DOX, compared to incubation of the cells with free DOX at different concentrations starting from 2 to 50 µM, which decrease the viability to 79% only. This could be attributed to the presence of the drug in a nano-system, and its diffusion into the cells is constant with no significant reflux effect from the cells to the drug. The developed Magnetite/silica/DOX could be a potential drug delivery system for highly toxic chemotherapeutic agents such as Doxorubicin. Moreover, the magnetite core could be used for hyperthermia by applying an alternating magnetic field (AMF), to the site of the particles within the tumor. Furthermore, the system can be used in enhancing the Magnetic Resonance Imaging (MRI), due to the presence of magnetite nanoparticles, which enhance the contrast in MRI and so, this type of particles could be used in Theragnostic (Therapeutic and diagnostics) with three effects: delivery of the chemotherapeutic agent, enhancing imaging by

Table 3. Effect of DOX at different concentrations on cell viability

	Cell viability %			
	DOX 2μM	DOX 10μM	DOX 20μM	DOX 50μM
MCF-7 / DOX	97.15±0.35	95.20±0.13	88.24±0.36	79.32±0.23
MCF-7 / DOX/ silica	86.34±0.29	81.14±0.56	71.27±0.12	55.35±84

Results expressed by mean ±SD

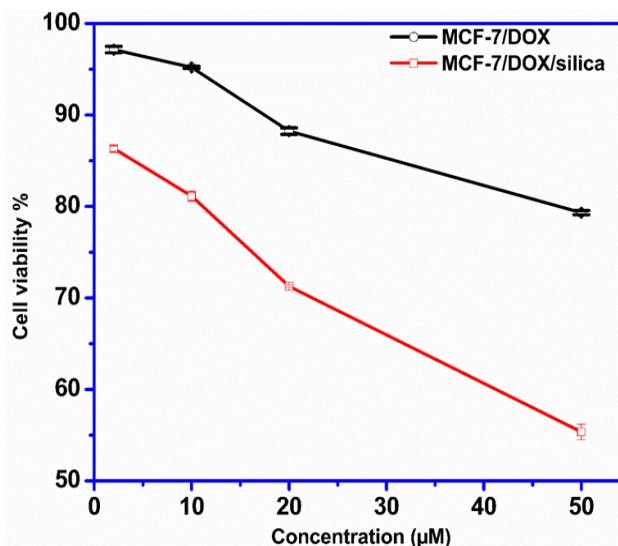


Figure 6. Evaluation of effect of adding free DOX at different concentrations (2-10 μM) on MCF7 cells either alone or in combination with DOX loaded DDS.

Table 4. Effect of DOX at different time interval on cell viability

	Cell viability %		
	Day 1	Day 4	Day 7
MCF-7 / Silica	99.24 ± 0.22	98.74 ± 0.18	98.53 ± 0.49
MCF-7 / DOX	82.12 ± 0.35	77.23 ± 0.24	71.45 ± 0.26
MCF-7 / DOX/ Silica	60.24 ± 0.24	52.15 ± 0.32	49.18 ± 0.72

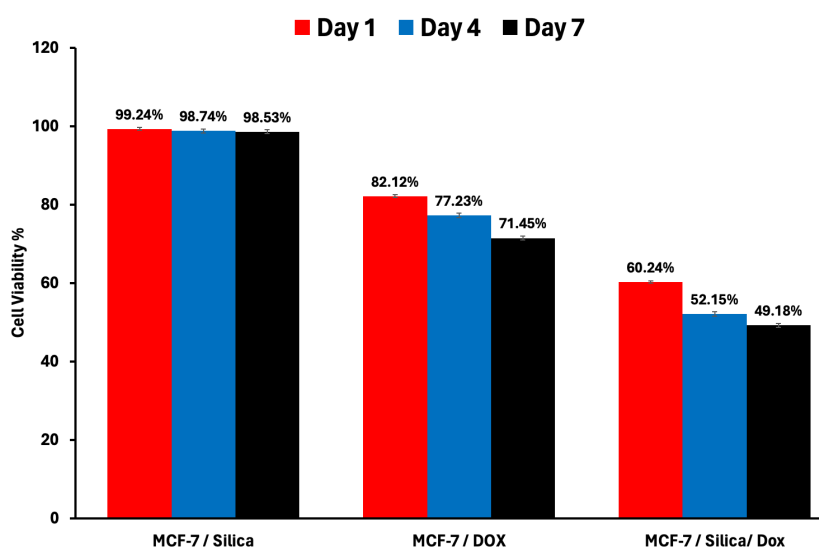


Figure 7. Effect of free DOX and DOX loaded delivery system at different time intervals on cell viability

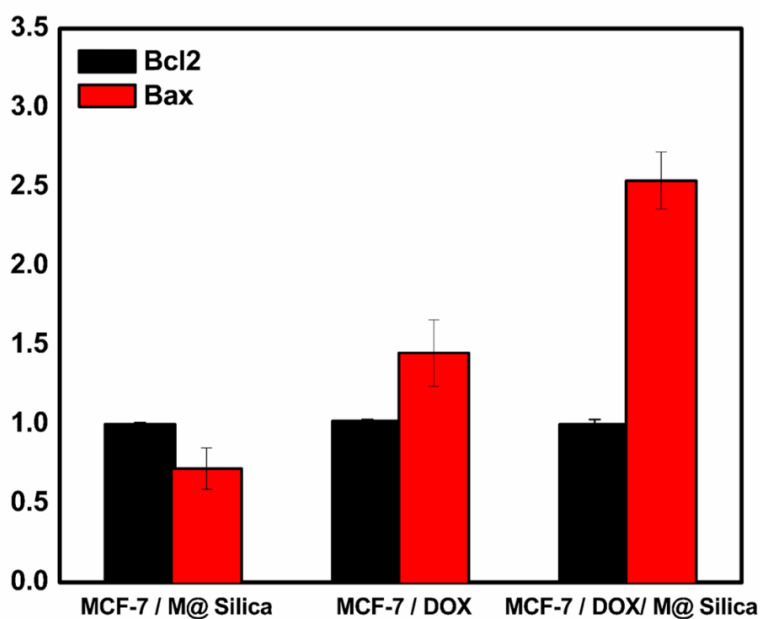


Figure 8. Effects of the studied drug on apoptotic process

Table 5. Real time PCR results

	MCF-7 /M@ Silica	MCF-7 / DOX	MCF-7 / DOX/ M@Silica
Bcl2	1±0.01	0.72±0.13*	1±0.03*#
Bax	1.02±0.01	1.45±0.21*	2.54±0.18*#

*P<0.05 when compared to MCF-7/ M@Silica group

#P<0.05 when compared to MCF-7 / DOX group

MRI and finally, hyperthermia, by using AMF which will lead to adsorption of these field by the particles and generate heat in-situ, and thus. Release of drug and heating the tumor cells leading to cell's death.

FUNDING:

We thank Tanta University Research Fund for financial support of this work through the Research Project of Code Tu: 02 – 19 - 04.

CONFLICT OF INTEREST

All authors declare that they have no conflicts of interest.

REFERENCES

- ABBAS, M., TAKAHASHI, M. & KIM, C. (2013). Facile sonochemical synthesis of high-moment magnetite (Fe₃O₄) nanocube. *Journal of nanoparticle research*, 15, 1-12.
- ABBAS, M., TORATI, S., LEE, C., RINALDI, C. & KIM, C. (2014). Fe₃O₄/SiO₂ core/shell nanocubes: novel coating approach with tunable silica thickness and enhancement in stability and biocompatibility. *J Nanomed Nanotechnol*, 5, 1-8.

- ABBAS, M., TORATI, S. R. & KIM, C. (2015). A novel approach for the synthesis of ultrathin silica-coated iron oxide nanocubes decorated with silver nanodots (Fe₃O₄/SiO₂/Ag) and their superior catalytic reduction of 4-nitroaniline. *Nanoscale*, 7, 12192-12204.

- ASAB, G., ZEREFFA, E. A. & ABDO SEGHNE, T. (2020). Synthesis of Silica-Coated Fe₃O₄ Nanoparticles by Microemulsion Method: Characterization and Evaluation of Antimicrobial Activity. *International Journal of Biomaterials*, (2020), 4783612.

- BANAEI, A., VOJUDI, H., KARIMI, S., BAHAR, S. & POURBASHEER, E. (2015). Synthesis and characterization of new modified silica coated magnetite nanoparticles with bisaldehyde as selective adsorbents of Ag (I) from aqueous samples. *RSC Advances*, 5, 83304-83313.

- CHEUNG, A. Y. & NEYZARI, A. (1984). Deep local hyperthermia for cancer therapy: external electromagnetic and ultrasound techniques. *Cancer Research*, 44, 4736s-4744s.

- DENG, Z., XIAO, Y., PAN, M., LI, F., DUAN, W., MENG, L., LIU, X., YAN, F. & ZHENG, H. (2016). Hyperthermia-triggered drug delivery from iRGD-modified temperature-sensitive liposomes

- enhances the anti-tumor efficacy using high intensity focused ultrasound. *Journal of Controlled Release*, 243, 333-341.
- ELLIS, E., ZHANG, K., LIN, Q., YE, E., POMA, A., BATTAGLIA, G., LOH, X. J. & LEE, T.-C. (2017). Biocompatible pH-responsive nanoparticles with a core-anchored multilayer shell of triblock copolymers for enhanced cancer therapy. *Journal of Materials Chemistry B*, 5, 4421-4425.
- FU, Y. & KAO, W. J. (2010). Drug release kinetics and transport mechanisms of non-degradable and degradable polymeric delivery systems. *Expert opinion on drug delivery*, 7, 429-444.
- GOUDA, R., BAISHYA, H. & QING, Z. (2017). Application of mathematical models in drug release kinetics of carbidopa and levodopa ER tablets. *J. Dev. Drugs*, 6, 1-8.
- HAKHEEM, A., ZAHID, F., ZHAN, G., YI, P., YANG, H., GAN, L. & YANG, X. (2018). Polyaspartic acid-anchored mesoporous silica nanoparticles for pH-responsive doxorubicin release. *Int J Nanomedicine*, 13, 1029-1040.
- JAIN, A., TIWARI, A., VERMA, A. & JAIN, S. K. (2018). Ultrasound-based triggered drug delivery to tumors. *Drug delivery and translational research*, 8, 150-164.
- KALANTARI, S., YOUSEFPOUR, M. & TAHERIAN, Z. (2017). Synthesis of mesoporous silica/iron oxide nanocomposites and application of optimum sample as adsorbent in removal of heavy metals. *Rare Metals*, 36, 942-950.
- KESHAVARZ, H., KHAVANDI, A., ALAMOLHODA, S. & NAIMI-JAMAL, M. R. (2020). pH-Sensitive magnetite mesoporous silica nanocomposites for controlled drug delivery and hyperthermia. *RSC Advances*, 10, 39008-39016.
- KORSMEYER, R. W., GURNY, R., DOELKER, E., BURI, P. & PEPPAS, N. A. (1983). Mechanisms of solute release from porous hydrophilic polymers. *International Journal of Pharmaceutics*, 15, 25-35.
- LAI, C.-Y., TREWYN, B. G., JEFTINIJA, D. M., JEFTINIJA, K., XU, S., JEFTINIJA, S. & LIN, V. S. Y. (2003). A Mesoporous Silica Nanosphere-Based Carrier System with Chemically Removable CdS Nanoparticle Caps for Stimuli-Responsive Controlled Release of Neurotransmitters and Drug Molecules. *Journal of the American Chemical Society*, 125, 4451-4459.
- LIU, Y., LI, Y., LI, X.-M. & HE, T. (2013). Kinetics of (3-aminopropyl) triethoxysilane (APTES) silanization of superparamagnetic iron oxide nanoparticles. *Langmuir*, 29, 15275-15282.
- MHLANGA, N. & RAY, S. S. (2015). Kinetic models for the release of the anticancer drug doxorubicin from biodegradable polylactide/metal oxide-based hybrids. *International journal of biological macromolecules*, 72, 1301-1307.
- MOORTHY, M. S., SUBRAMANIAN, B., PANCHANATHAN, M., MONDAL, S., KIM, H., LEE, K. D. & OH, J. (2017). Fucoidan-coated core-shell magnetic mesoporous silica nanoparticles for chemotherapy and magnetic hyperthermia-based thermal therapy applications. *New Journal of Chemistry*, 41, 15334-15346.
- NARAYANASWAMY, V., AL-OMARI, I. A., KAMZIN, A. S., GOPI, C. V. M., KHALEEL, A., ALAABED, S., ISSA, B. & OBAIDAT, I. M. (2022). Exchange bias, and coercivity investigations in hematite nanoparticles. *AIMS Materials Science*, 9, 71-84.
- PATTNAIK, A. (2011). *Synthesis and characterization of amine-functionalized magnetic silica nanoparticle*.
- QIAO, B., WANG, T.-J., GAO, H. & JIN, Y. (2015). High density silanization of nano-silica particles using γ -aminopropyltriethoxysilane (APTES). *Applied Surface Science*, 351, 646-654.
- SHAHABI, S., DÖSCHER, S., BOLLHORST, T., TRECCANI, L., MAAS, M., DRINGEN, R. & REZWAN, K. (2015). Enhancing cellular uptake and doxorubicin delivery of mesoporous silica nanoparticles via surface functionalization: effects of serum. *ACS applied materials & interfaces*, 7, 26880-26891.
- SHAWKY, S., ABO-ALHASSAN, A., LILL, H., BALD, D. & EL-KHAMISY, S. (2016)a. Efficient Loading and Encapsulation of Anti-Tuberculosis Drugs using Multifunctional Mesoporous Silicate Nanoparticles. *J Nanosci Curr Res* 1: 103. doi: 10.4172/2572-0813.1000103 Page 2 of 9 Volume 1 • Issue 1 • 1000103 *J Res Development*, an open access journal ISSN: 2311-3278 [14, 16-20](Figure 1). vitro.
- SHAWKY, S. M., ABO-ALHASSAN, A. A., LILL, H., BALD, D., EL-KHAMISY, S. & EBEID, E. Z. (2016)b. Efficient Loading and Encapsulation of Anti-Tuberculosis Drugs using Multifunctional Mesoporous Silicate Nanoparticles. *J Nanosci Curr Res*, 1, 9.
- SHAWKY, S. M., GUIRGIS, B. S. & AZZAZY, H. M. (2014). Detection of unamplified HCV RNA in serum using a novel two metallic nanoparticle platform. *Clin Chem Lab Med*, 52, 565-72.
- SLOWING, I. I., TREWYN, B. G., GIRI, S. & LIN, V. S.-Y. (2007). Mesoporous Silica Nanoparticles for Drug Delivery and Biosensing Applications. *Advanced Functional Materials*, 17, 1225-1236.
- STRAND, M. (2016). *Amino-Functionalized Magnetic Nanoparticles for Extraction of Naphthenic Acids*. NTNU.
- SUN, L., HU, S., SUN, H., GUO, H., ZHU, H., LIU, M. & SUN, H. (2015). Malachite green adsorption onto

- $\text{Fe}_3\text{O}_4@\text{SiO}_2\text{-NH}_2$: isotherms, kinetic and process optimization. *RSC Advances*, 5, 11837-11844.
- T. CHATZĒĪŌANNOU(1993). *Quantitative Calculations in Pharmaceutical Practice and Research*, New York, VCH.
- T.M. EL-ALAILY M.K. EL-NIMR , S. A. S., M.M. KAMEL ,T.M. MEAZ, S.T. ASSER (2015). construction and celebration of low cost and fully automated vibrating sample magnetometer *journal of magnetization and magnetic material*
- TASCIOTTI, E., LIU, X., BHAVANE, R., PLANT, K., LEONARD, A. D., PRICE, B. K., CHENG, M. M. C., DECUZZI, P., TOUR, J. M., ROBERTSON, F. & FERRARI, M. (2008). Mesoporous silicon particles as a multistage delivery system for imaging and therapeutic applications. *Nature Nanotechnology*, 3, 7.
- TORNEY, F., TREWYN, B. G., LIN, V. S. Y. & WANG, K. (2007). Mesoporous silica nanoparticles deliver DNA and chemicals into plants. *Nature Nanotechnology*, 2, 295-300.
- ULLAH, R., DEB, B. K. & MOLLAH, M. Y. A. (2014). Synthesis and characterization of silica coated iron-oxide composites of different ratios. *Int J Compos Mater*, 4, 135-145.
- UNSOY, G., KHODADUST, R., YALCIN, S., MUTLU, P. & GUNDUZ,U.(2014).Synthesis of Doxorubicin loaded magnetic chitosan nanoparticles for pH responsive targeted drug delivery. *European Journal of Pharmaceutical Sciences*, 62, 243-250.
- WATERMANN, A. & BRIEGER, J. (2017). Mesoporous silica nanoparticles as drug delivery vehicles in cancer. *Nanomaterials*, 7, 189.
- WHO. (2021)a. *Fact sheets: Cancer* [Online]. WHO. Available: <https://www.who.int/news-room/fact-sheets/detail/cancer> [Accessed July 2021 2021].
- WHO. (2021)b. *World fact sheets* [Online]. Available: <https://gco.iarc.fr/today/data/factsheets/populations/900-world-fact-sheets.pdf> [Accessed July 2021 2021].
- XIAO, Q. & XIAO, C. (2009). Preparation and characterization of silica-coated magnetic-fluorescent bifunctional microspheres. *Nanoscale research letters*, 4, 1078-1084.
- YAN, J., XU, X., ZHOU, J., LIU, C., ZHANG, L., WANG, D., YANG, F. & ZHANG, H. (2020). Fabrication of a pH/Redox-Triggered Mesoporous Silica-Based Nanoparticle with Microfluidics for Anticancer Drugs Doxorubicin and Paclitaxel Codelivery. *ACS Applied Bio Materials*, 3, 1216-1225.
- YU, X. & ZHU, Y. (2016). Preparation of magnetic mesoporous silica nanoparticles as a multifunctional platform for potential drug delivery and hyperthermia. *Science and Technology of advanced MaTerialS*, 17, 229-238.
- ZADA, A., PEEK, M., AHMED, M., ANNINGA, B., BAKER, R., KUSAKABE, M., SEKINO, M., KLAASE, J., TEN HAKEN, B. & DOUEK, M. (2016). Meta-analysis of sentinel lymph node biopsy in breast cancer using the magnetic technique. *British journal of surgery*, 103, 1409-1419.